

Article

Interaction of Arylidenechromanone/Flavanone Derivatives with Biological Macromolecules Studied as Human Serum Albumin Binding, Cytotoxic Effect, Biocompatibility Towards Red Blood Cells

Angelika A. Adamus-Grabicka ¹, Magdalena Markowicz-Piasecka ² , Michał B. Ponczek ³, Joachim Kusz ⁴, Magdalena Małecka ⁵, Urszula Krajewska ⁶ and Elzbieta Budzisz ^{1,*}

¹ Department of Cosmetic Raw Materials Chemistry, Faculty of Pharmacy, Medical University of Lodz, ul Muszynskiego 1, 90-151 Lodz, Poland; angelika.adamus@umed.lodz.pl

² Laboratory of Bioanalysis, Department of Pharmaceutical Chemistry, Drug Analysis and Radiopharmacy, Medical University of Lodz, Muszyńskiego1, 90-151 Lodz, Poland; magdalena.markowicz@umed.lodz.pl

³ Department of General Biochemistry, Faculty of Biology and Environmental Protection, University of Lodz, Pomorska 141/143, 90-236 Lodz, Poland; michal.ponczek@biol.uni.lodz.pl

⁴ Institute of Physics, University of Silesia, Uniwersytecka 4, 40-007 Katowice, Poland; joachim.kusz@us.edu.pl

⁵ Department of Physical Chemistry, Theoretical and Structural Chemistry Group, Faculty of Chemistry, University of Lodz, Pomorska 163/165, 90-236 Lodz, Poland; magdalena.malecka@chemia.uni.lodz.pl

⁶ Department of Pharmaceutical Biochemistry and Molecular Diagnostics, Faculty of Pharmacy, Medical University of Lodz, Muszynskiego 1, 90-151 Lodz, Poland; urszula.krajewska@umed.lodz.pl

* Correspondence: elzbieta.budzisz@umed.lodz.pl; Tel.: +42-272-55-95

Received: 25 October 2018; Accepted: 28 November 2018; Published: 1 December 2018



Abstract: The aim of this study was to determine the cytotoxic effect of 3-arylidenechromanone (**1**) and 3-arylidene flavanone (**2**) on HL-60 and NALM-6 cell lines (two human leukemia cell lines) and a WM-115 melanoma cell line. Both compounds exhibited high cytotoxic activity with higher cytotoxicity exerted by compound **2**, for which IC₅₀ values below 10 μM were found for each cell line. For compound **1**, the IC₅₀ values were higher than 10 μM for HL-60 and WM-115 cell lines, but IC₅₀ < 10 μM was found for the NALM-6 cell line. Both compounds, at the concentrations close to IC₅₀ (concentration range: 5–24 μM/L for compound **1** and 6–10 μM/L for compound **2**), are not toxic towards red blood cells. The synthesized compounds were characterized using spectroscopic methods ¹H- and ¹³C-NMR, IR, MS, elemental analysis, and X-ray diffraction. The lipophilicity of both synthesized compounds was determined using an RP-TLC method and the log*P* values found were compared with the theoretical ones taken from the Molinspiration Cheminformatics (miLog*P*) software package. The mode of binding of both compounds to human serum albumin was assessed using molecular docking methods.

Keywords: synthesis; crystal structure; cytotoxic effect; benzoflavanone/chromanone derivatives; erythrotoxicity

1. Introduction

Flavonoids constitute a large group of natural and synthetic polyphenolic compounds with a wide range of antioxidant, anti-allergic, anti-inflammatory, anti-microbial, anti-coagulant, anti-cholesterol, or anti-cancer activities. These properties often depend on unknown structure-related interactions with nucleic acids and proteins [1,2]. Due to their antioxidant properties, flavonoids interfere with the initiation, promotion, and progression of cancer. Flavonoids modulate the activities of various enzymes and receptors involved in several signal transduction pathways, thus affecting cell proliferation,

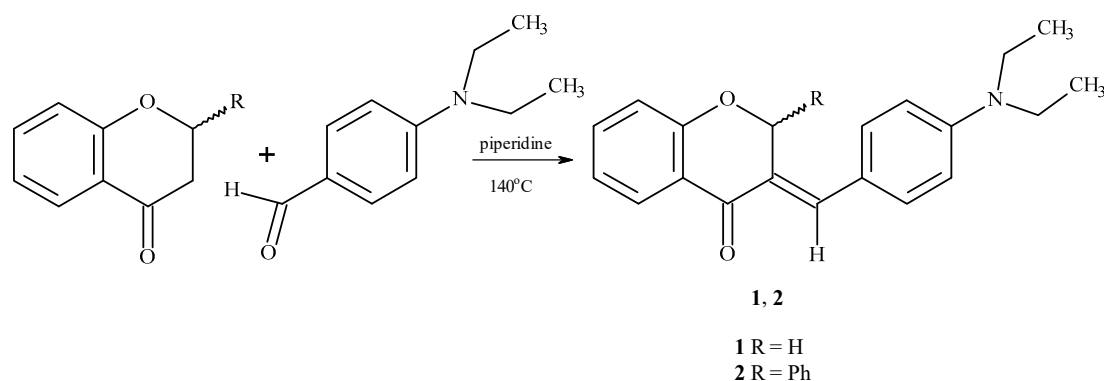
apoptosis, as well as the processes of inflammation, angiogenesis, and metastasis [3]. Due to their multidirectional mechanisms of action, flavonoids are promising candidates for novel anti-cancer agents and are being extensively investigated for the treatment of neoplastic diseases [3–5]. For instance, it was found that, in vivo, quercetin exerts a chemo-preventive effect on prostate cancer (reduces the cell viability) by downregulating the activity of pro-proliferative and anti-apoptotic proteins [6]. Additionally, synthetic derivatives of naturally occurring flavonoids (e.g., derivatives of chroman-4-one and tiorchmane-4-one [7]) are studied for their anti-cancer properties.

3-arylidenechroman-4-ones, a group of naturally occurring homoisoflavones, can be obtained by the condensation of aryl aldehydes with chroman-4-ones (chromanones). It was first synthesized by Robinson and co-workers in the early twenties by condensation of chromanon with the corresponding aryl aldehyde using alcoholic potassium hydroxide as a catalyst [8]. Other catalysts have also been proposed. In 1979, Levai and Schag synthesized *E*-3-arylidenechroman-4-ones using piperidine as a catalyst, while piperidine has also been successfully used as a catalyst for the synthesis of 3-benzylidenechroman-4-ones and 3-benzylidene flavanones [9,10]. In recent years, Kupcewicz and co-authors [11], as well as our group [12], have investigated the cytotoxicity of *E* and *Z* isomers of 3-arylidene flavanone derivatives. Those compounds exhibit high cytotoxicity with $IC_{50} < 10 \mu M$. However, no significant difference in cytotoxicity of *E* and *Z* isomers was observed. In this study the structure of (E)-3-(4-*N,N*-diethylaminobenzylidene)chroman-4-one (**1**) and (E)-3-(4-*N,N*-diethylaminobenzylidene)-2-phenylchroman-4-one (**2**) was elucidated using single crystal X-ray diffraction (XRD), MS, and NMR spectroscopy. Despite being first synthesized in the 1970s [9,10], compound **1** was presented as an American patent in 2008 [13] and compound **2** was synthesized in 1993 by Pijewska [14], but their cytotoxic activity has never been studied. The cytotoxicity of 3-arylidenechromanone and flavanone substituted with *p*-aminodiethyl on C3 atom in benzene ring has also been investigated. In addition, the lipophilicity ($miLogP$) of **1** and **2** and their activity against red blood cells were determined. The mode of binding to human serum albumin (HSA, a protein important in binding and transport of various drugs [15]) has also been elucidated by molecular docking methods. Computational docking of ligand binding to target proteins is often performed as part of Structure-Based Virtual Screening used in drug discovery and this approach enables molecular interactions with macromolecules to be predicted [16]. We also assess the lipophilicity and their influence on the various biological properties.

2. Results and Discussion

2.1. Chemistry

The cytotoxic effects of *E* and *Z*-isomers of benzylidene flavanone are compared in a previous paper [11]. The current paper compares the cytotoxicity of chromanone and flavanone derivatives. (E)-3-(4-*N,N*-diethylaminobenzylidene)chroman-4-one (**1**) and (E)-3-(4-*N,N*-diethylaminobenzylidene)-2-phenylchroman-4-one (**2**) synthesized, as described previously [14] (Scheme 1).



Scheme 1. Synthesis of compounds **1** and **2** (when R = H or Ph).

Both compounds were fully characterized using IR, $^1\text{H-NMR}$, $^{13}\text{C-NMR}$, and MS spectroscopy and elemental analysis.

The ν (C=O) band for compound **1** was observed at 1663 cm^{-1} , and bands typical for aromatic rings were noted at 1600 , 1584 , and 1524 cm^{-1} . An IR spectrum of **2** showed a band at 1654 cm^{-1} and typical bands for the aromatic rings at 1603 , 1559 , and 1524 cm^{-1} . The $^1\text{H-NMR}$ spectrum for compound **1** revealed the presence of a triplet from $-\text{CH}_3$ protons at 1.12 ppm and a quartet around 3.42 ppm corresponding to the CH_2 protons (see Figure S1). A singlet for $=\text{C-H}$ was observed at $\delta\ 5.45\text{ ppm}$. At $\delta\ 6.75\text{ ppm}$, a doublet for the C2-H protons was observed. The characteristic signals $\delta\ 7.02\text{--}7.85\text{ ppm}$ correspond to the aromatic protons. The $^1\text{H-NMR}$ spectrum for compound **2** revealed the presence of a triplet from $-\text{CH}_3$ protons at 1.12 ppm (see Figure S2). A quartet corresponding to the CH_2 protons was observed at $\delta\ 3.36\text{ ppm}$. At $\delta\ 6.70\text{ ppm}$ a singlet for C2-H protons was noted. The signals at $\delta\ 6.81\text{--}7.79\text{ ppm}$ correspond to the aromatic protons. A singlet for $=\text{C-H}$ was observed at $\delta\ 7.94\text{ ppm}$. In the $^{13}\text{C-NMR}$ spectrum for compound **1**, the characteristic CH_3 group signal was found at $\delta\ 12.9\text{ ppm}$, while the $-\text{CH}_2$ group was observed at 44.3 ppm (see Figure S1a). The C2-H carbon signal was observed at $\delta\ 78.1\text{ ppm}$. At $\delta\ 181.0\text{ ppm}$, a signal for C=O was observed. In addition the $^{13}\text{C-NMR}$ spectrum showed the presence of CH_{arom} and C_{arom} signals, which were expected for the postulated structure of (E)-3-(4-*N,N*-diethylaminobenzylidene)chroman-4-one. For compound **2**, the $^{13}\text{C-NMR}$ spectrum showed the presence of signals located at $\delta\ 12.9\text{ ppm}$, attributed to a CH_3 group and at $-\text{CH}_2$ group at $\delta\ 44.3\text{ ppm}$ (see Figure S2a). In the $^{13}\text{C-NMR}$ spectrum, a $-\text{C}=\text{O}$ related resonance was found at $\delta\ 181.2\text{ ppm}$, those for CH_{arom} and C_{arom} were also found. The mass spectrum revealed a band in **1** at $m/z = 308.2$, indicating $([\text{M} + \text{H}]^+)$, and in **2**, at $m/z = 384$, indicating the presence of an $[\text{M} + \text{H}]$ ion.

2.2. Molecular Structures

The molecular structure of compound **1** and **2** is presented in (Figure 1). A molecule of **1** consists of two condensed rings (benzene and pyran) with 4-*N,N*-diethylaminobenzylidene substituent in position 3 of the benzopyran ring. It crystallizes in a triclinic system in a $\text{P}\bar{1}$ space group with two molecules in the asymmetric unit. The two independent molecules demonstrate different geometries in the arrangement of the 4-*N,N*-diethylaminobenzylideno moiety with respect to the main benzopyran skeleton. In molecule A, it is nearly planar with dihedral angles C3-C11-C12-C13 $-8.32(1)$ and C3-C11-C12-C17 $172.80(1)^\circ$, while in molecule B, it is rotated by about 35° with the dihedral angles C53-C61-C62-C63 of $-35.41(1)^\circ$ and C53-C61-C62-C67 of $148.31(1)$. Moreover, the pyran rings slightly vary in conformation. In molecule A, the pyran ring adopts an envelope conformation with puckering ring parameters [11] $Q = 0.300(2)\text{ \AA}$, $\varphi = 57.0(3)$, $\theta = 62.5(2)^\circ$, and the asymmetry parameter [12] $\Delta C_s(\text{C}2) = 2.75(1)^\circ$. The corresponding parameters for the pyran ring in the molecule B are: $Q = 0.451(2)\text{ \AA}$, $\varphi = 44.9(3)^\circ$, $\theta = 64.6(2)^\circ$, and the asymmetry parameter

$\Delta C_2(O51-C52) = 14.0(1)^\circ$, which indicates a screw-boat conformation. Valkonen [17] notes that, in the structure of (E)-3-(4-(dimethylamino)benzylidene)-2,3-dihydro-4H-chromen-4-one, there are also two independent molecules crystallizing in an asymmetric unit of the Pc group. The benzopyran skeleton and the 4-dimethylaminobenzylideno moiety are not planar with dihedral angles of $24.96(2)^\circ$ and $49.53(2)^\circ$ for molecules A and B, respectively. For the C6-C10-C2-C12/C9 and C22-C2)-C19-C21/C31, the corresponding torsion angles of $32.65(2)^\circ/149.33(2)^\circ$, $-29.42(2)^\circ$, and $156.30(2)^\circ$ were reported. However, the pyran rings adopt a similar conformation: An envelope conformation with the puckering ring parameters [18] $Q = 0.349(2)\text{\AA}$, $\varphi = 309.1(2)$, $\theta = 58.6(2)^\circ$, the asymmetry parameter [19] $\Delta C_s(C4) = 7.30(1)^\circ$ for O1/C5/C6/C3/C4/C1 ring, a screw boat conformation with $Q = 0.405(2)\text{\AA}$, $\varphi = 143.0(2)$, $\theta = 113.5(2)^\circ$, and the asymmetry parameter [20] $\Delta C_2(C24-C29) = 4.91(1)^\circ$ for the O4/C28/C22/C29/C24/C26 ring

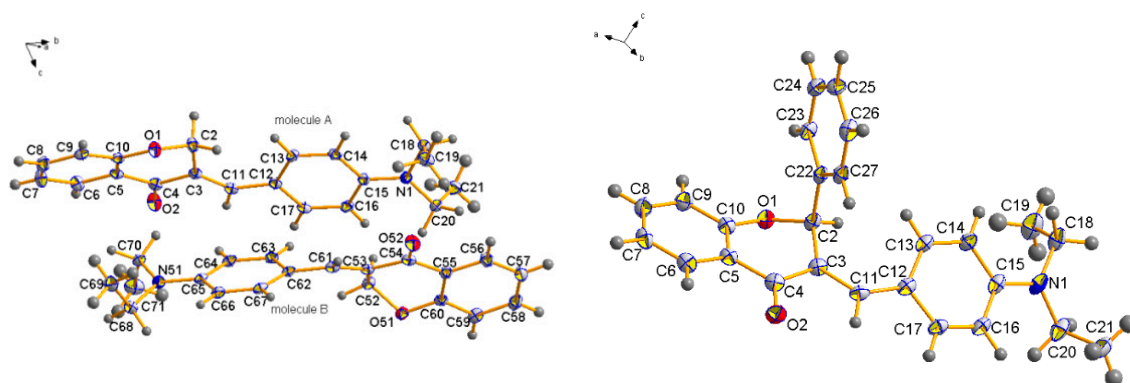


Figure 1. Molecular structures of **1** and **2**, with atom-numbering schemes. The anisotropic displacement parameters are shown at the 30% probability level. Hydrogen atoms are drawn as spheres of arbitrary radius.

The crystal packing of **1** is dominated by C-H ... O and C-H ... π interactions (Figure 2). The molecules A and B are linked by C8-H8 ... O2 ($-1 + x, y, z$) and C67-H67 ... O51 ($-1 + x, y, z$) hydrogen bonds, respectively, forming two ribbons, which are further coupled by C56-H56 ... O2 ($x, 1y, z$) hydrogen bond that produces a layer. Other C52-H52 ... O51 ($1 - x, 1 - y, 1 - z$) interactions are responsible for creating the 3-D network of hydrogen bonds connecting two layers. In both molecules, the intramolecular hydrogen bonds C11-H11 ... O2 and C61-H61 ... O52 are observed (Table 1).

Table 1. Hydrogen-bonding geometries (in \AA , $^\circ$) for structure **1**.

	D-H	H...A	D...A	D-H...A
C11-H11 ... O2	0.93	2.35	2.768 (2)	107
C61-H61 ... O52	0.93	2.45	2.811 (2)	103
C8-H8 ... O2 ⁱ	0.93	2.63	3.198 (2)	120
C67-H67 ... O51 ⁱ	0.93	2.59	3.409 (2)	147
C52-H52A ... O51 ⁱⁱ	0.97	2.60	3.274 (2)	126
C56-H56 ... O2 ⁱⁱⁱ	0.93	2.70	3.498 (2)	144
C2-H2B ... Cg3 ^{iv}	0.97	2.87	3.717 (2)	147
C16-H16 ... Cg7 ^v	0.93	2.90	3.726 (2)	148
C21-H21C ... Cg2 ^{iv}	0.96	2.95	3.712 (2)	137
C59-H59 ... Cg7 ⁱⁱ	0.93	2.71	3.545 (2)	150
C69-H69B ... Cg6 ^{vi}	0.96	2.93	3.645 (2)	132

Symmetry codes: (i): $-1+x, y, z$; (ii): $1 - x, 1 - y, 1 - z$, (iii): $x, 1+y, z$ (iv): $1 - x, 1 - y, -z$, (v) $1 + x, y, z$, (vi): $-x, 1 - y, 1 - z$ Cg2, Cg3, Cg6, Cg7—centroids of C5/C6/C7/C8/C9/C10, C12/C13/C14/C15/C16/C17, C55/C56/C57/C58/C59/C60, and C62/C63/C64/C65/C66/C67 rings.

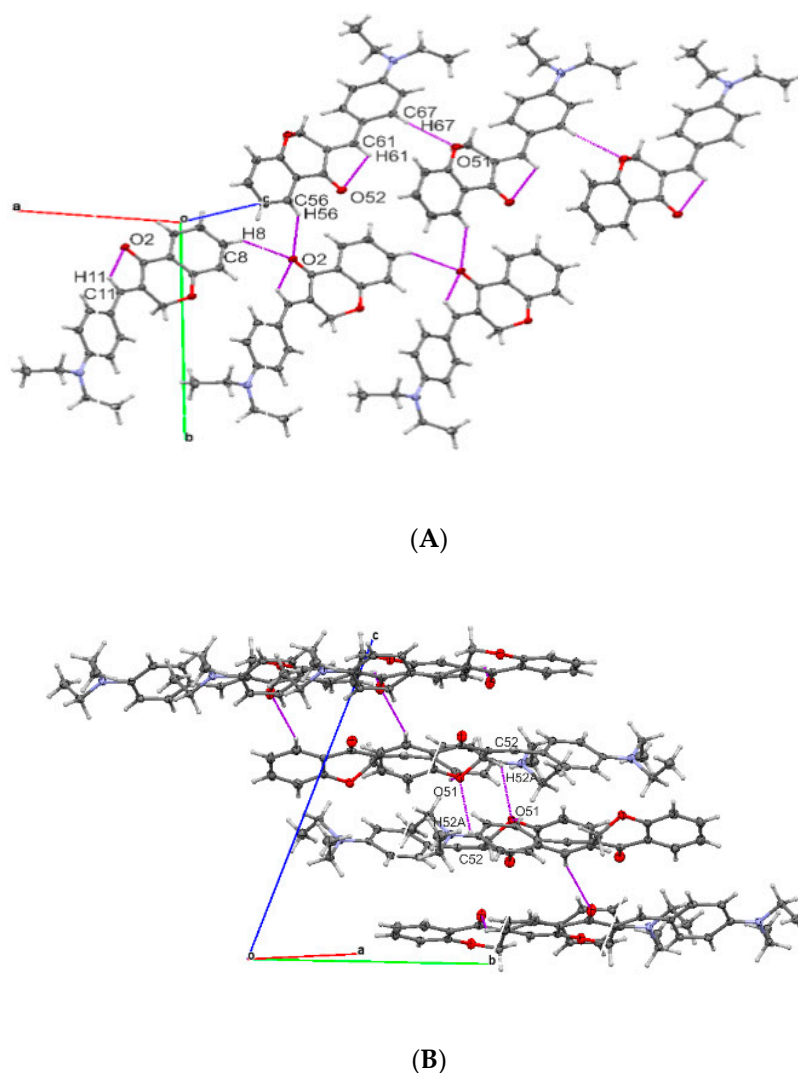


Figure 2. Chains and layer of (1) supported by C-H...O hydrogen bonds (A) that build a 3-D network of hydrogen bonds (B) and view of equivalent molecules linked by hydrogen bonds (top right).

Compound **2** crystallizes in a monoclinic system in the $P2_1/n$ space group. The main skeleton of the molecule consists of fused benzene and pyran rings, the latter bears a phenyl ring at position 2 and a 4-*N,N*-diethyloaminobenzylidene substituent at position 3. The C-2 phenyl ring is perpendicular, while the aminobenzylidene substituent is nearly co-planar to the pyran ring. The corresponding dihedral angles are: C3-C2-C22-C27 $-13.0(2)^\circ$ and C3-C11-C12-C13 $19.2(3)^\circ$, while the dihedral angle between the best planes of those phenyl rings is $83.7(2)^\circ$. In molecule **2**, the pyran ring adopts a distorted half-boat conformation with the puckering ring parameters [21] $Q = 0.411(2)\text{\AA}$, $\varphi = 220.6(3)^\circ$, $\theta = 119.2(2)^\circ$, and the asymmetry parameter [22] $\Delta C_2(O1-C2) = 7.80(2)^\circ$.

In comparison to previously investigated similar molecules [11], the appropriate torsion angles are: $-16.4(2)^\circ$ and $32.5(2)^\circ$ with a dihedral angle observed between the best planes of phenyl rings $52.8(1)^\circ$. The pyran ring also adopts a nearly half boat conformation with puckering parameters [20] $Q = 0.341(2)\text{\AA}$, $\varphi = 226.1(3)^\circ$, and $\theta = 120.3(2)^\circ$.

In the crystal packing of **2**, hydrogen bonded dimers are observed, and these are stabilized by C16-H16...O2 interactions ($1-x, 1-y, -z$) (Figure 3). The intramolecular C11-H11...O2 hydrogen bond is also observed similar to compound **1**. The crystal packing is also enhanced by C-H... π interactions (Table 2).

2.3.2. Rbcs Lysis Assay

In studies on the integrity of the erythrocyte membrane, statistically significant results in comparison with saline control were obtained for compound 2 at the highest concentrations tested (9 and 10 $\mu\text{mol/L}$) (Figure 4), which implies that compounds at these concentrations contributed to red blood cell breakdown. However, the values of hemolysis did not exceed 10%, which is considered to be a clinically important threshold of cytotoxicity [24].

In contrast, compound 1 did not lead to any significant increase in the hemolysis rate, therefore, it might be concluded that both examined compounds do not show adverse effects on the integrity of the red blood cells (RBCs) membrane over the entire concentration range.

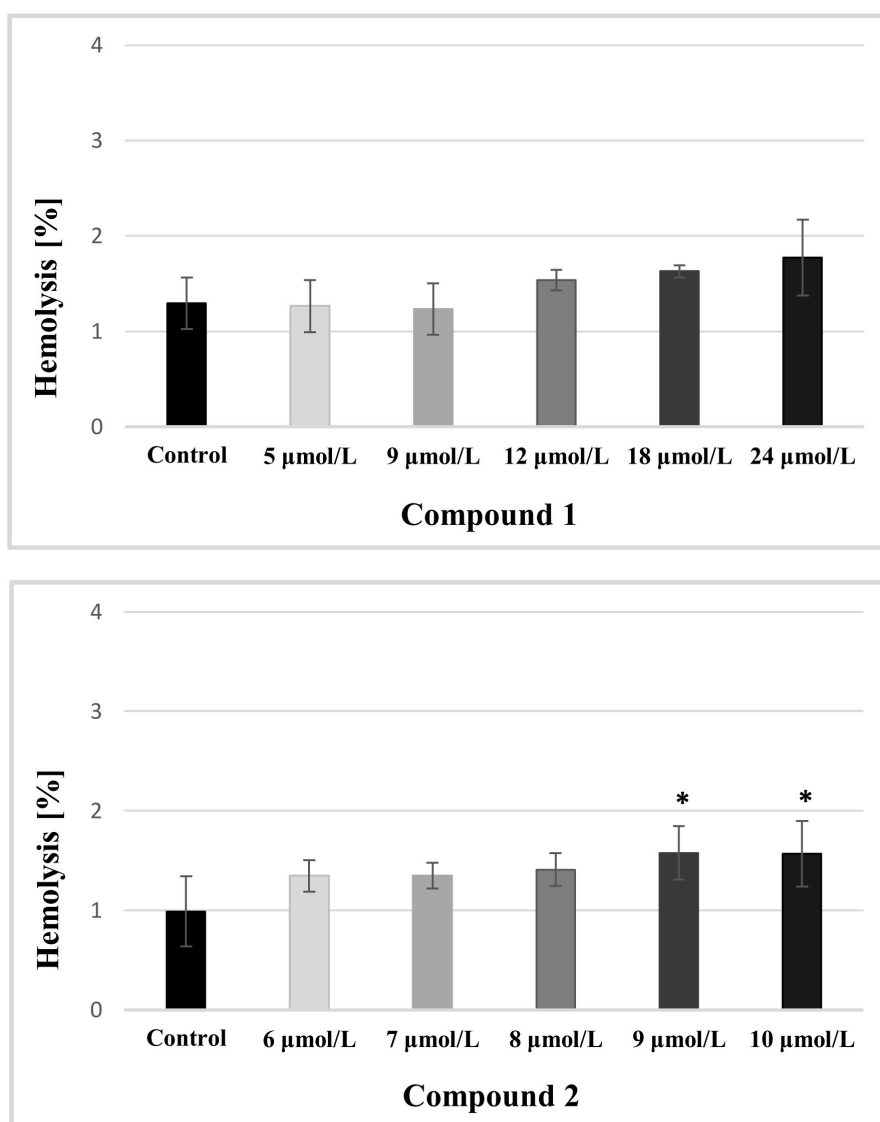


Figure 4. The effects of compound 1 and 2 on the integrity of the erythrocyte membrane. The results are presented as the percentage of hemolysis obtained from the interaction of studied compounds with 2% red blood cells (RBCs) suspension, compared to the positive control Triton X-100 at 0.2% (100% hemolysis) (mean \pm SD; $n = 4$), * $p < 0.05$ vs. control.

2.3.3. RBCs Morphology

When a drug molecule is administered intravenously a series of interactions with blood cells might be initiated. The effects of **1** and **2** on the morphology of erythrocytes were visualized by microscope studies (Figure 5).

Both tested compounds **1** and **2**, contributed to the formation of echinocytes. Echinocytes accounted for the major part of erythrocytes when 24 $\mu\text{mol/L}$ compound **1** was applied. As presented in Figure 5, compound **2** led to the formation of echinocytes over the entire concentration range, however, the percentage of this erythrocyte form differed according to the concentration of **2**. The transformation of biconcave erythrocytes to echinocytes occurs naturally in blood vessels, and could be also seen in control samples. It has been proved that echinocytosis is a reversible transformation caused by various chemical and physical factors including increased ion strength, alkaline pH, and decreased in adenosine triphosphate (ATP) level [25].

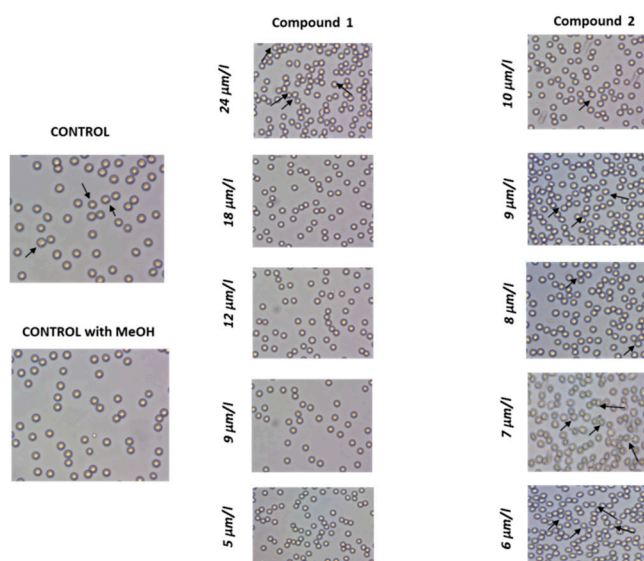


Figure 5. The microscope images of erythrocytes treated with compounds **1** and **2**. 2% erythrocyte suspension was treated at 37 °C for 60 min with indicated concentrations of compound **1** and **2**. Representative phase-contrast images are shown (magnification of 400 times). Black arrows indicate echinocytes.

2.4. Computational Studies

When drugs circulate in blood, they interact with biological macromolecules such as plasma proteins; these albumins constitute the majority and are important in the pharmacokinetics of medicines. For derivatives **1** and **2**, tenfold blind experiments of docking to HSA were performed to establish locations of their binding sites and the strength of the hypothetical interactions. The compounds were found to bind through hydrophobic interactions, **1** in four different places (near the cleft site, at the IB and FA1 sites, above the IIA—drug site and some additional atypical place) with average ΔG° -7.5 kcal/mol, whereas **2**, only in the IB FA1 site with average ΔG° -9.5 kcal/mol (Figure 6A,B). This single binding most likely resulted from the presence of an additional phenyl ring at the C2 position. The $\pi \dots \pi$ stacking was an important interaction between phenyl rings of the docked compounds and the aromatic side chains of tyrosine and phenylalanine. In the IB FA1 site, the aromatic rings of Tyr138 and 4-diethylaminobenzylidene substituent were parallel and were only slightly offset from each other with a distance between 4.4 and 4.5 Å. The phenyl ring in position 2 was located between the phenyl rings of Tyr138 and Phe125. The pyran ring was located between the phenyl ring of Phe125 and the aliphatic chain of Lys137 (Figure 6C,D). In contrast, compound **1** was located in the IB FA1 site inversely and showed less potent hydrophobic interactions.

The rings of the 4-*N,N*-diethyloaminobenzylidene substituent and Tyr138 were arranged in a parallel orientation, but were much more offset. The pyran ring was perpendicular to the phenyl ring of Tyr140 with a distance greater than 5 Å. His247 and Tyr30 were isolated with the distance greater than 20 Å. For compound **1**, mainly hydrophobic interactions with the aliphatic amino acid residues were observed in the other binding sites, and in the case of the cleft site, an oblique interaction between the pyran ring with the Tyr452 phenyl ring could be possible within a distance of 3.6 Å. In one atypical place, a similar interaction with the imidazole ring of His146 could take place within a distance of 3.3 Å. No specific hydrogen bonds were detected for either compounds.

To predict other properties of compounds **1** and **2**, the Molinspiration web tool was used and the drug descriptors were counted. For the Molinspiration GPCR ligand, Ion channel modulator, Kinase inhibitor, Nuclear receptor ligand, enzyme inhibitor and protease inhibitor bioactivity the scores were < zero or near zero, indicating that the compounds were not typical inhibitors or agonists of the listed types of proteins. Ligand efficiencies (LE) for derivatives calculated from computationally estimated ΔG° and known number of heavy atoms, theoretical $\log P$ and $\log P/LE$ (LELP), divided by the predicted number of binding sites were different for two compounds, but were still within the range of drug-likeness (Table 4).

The experimental lipophilicity of the synthesized compounds was determined using RP-TLC: $\log P$ values 3.43 was obtained for compound **1** and 5.69 for compound **2**. Theoretical values of lipophilicity were calculated using Molinspiration Cheminformatics (miLog P):miLog P 4.47 was obtained for **1** and 6.05 for **2**, i.e., similar to those obtained experimentally. Greater values of experimental and theoretical lipophilicity were noted for **2** because of the presence of the phenyl ring in the C2 position. Thus, molecular docking and Molinspiration predictions suggest that **1** and **2** have greater hydrophobicity than **1**, but also indicate potential specificity influence of an additional phenyl ring.

Table 4. Molinspiration bioactivity score and drug likeliness. H.A., the number of heavy atoms, n, number of binding sites, and LE, Ligand Efficiency ($-\Delta G^\circ/H.A.$), LELP ($\log P/LE$).

Compound	Bioactivity Score	H.A.	n	ΔG° Bind (kcal/mol)	$\log P$ (<i>exp</i>)	miLog P	LE	LELP
1	GPCR ligand −0.15	23	4	−7.5	3.43	4.47	0.33	13.55
	Ion channel modulator −0.30							
	Kinase inhibitor −0.30							
	Nuclear receptor ligand −0.04							
	Protease inhibitor −0.38							
	Enzyme inhibitor −0.11							
2	GPCR ligand −0.04	29	1	−9.1	5.69	6.05	0.31	19.52
	Ion channel modulator −0.32							
	Kinase inhibitor −0.26							
	Nuclear receptor ligand 0.03							
	Protease inhibitor −0.31							
Enzyme inhibitor −0.08								

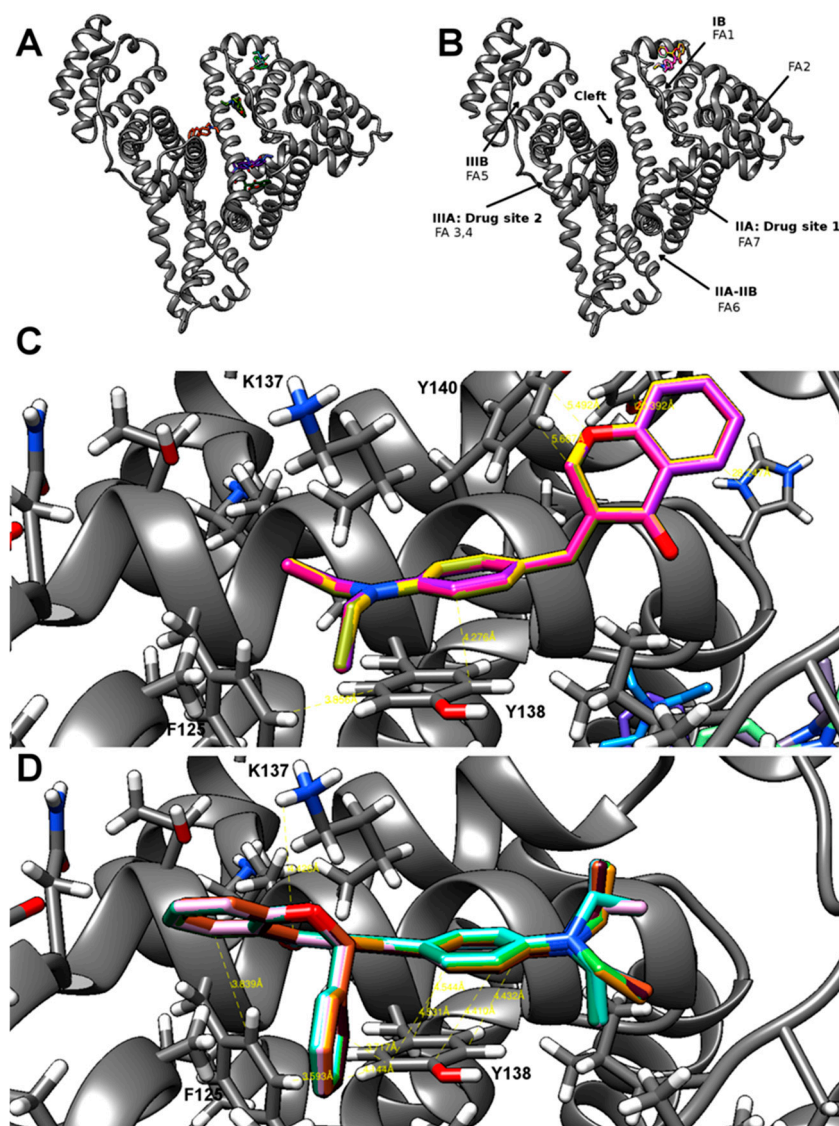


Figure 6. Tenfold blind docking of derivative **1** and **2** to HSA. Ribbon-stick models present the docking of derivatives (sticks) I-A, C and II-B, D to 1E7I human albumin structure (ribbon) with binding affinity energy (ΔG°) -7.5 ± 0.2 and -9.1 ± 0.1 (kcal/mol \pm SD), respectively. C, D are the zoom of IB FA1 binding site area, distances marked by yellow dashed lines.

3. Materials and Methods

The second compound **2** was synthesized according to Pijewska [14]. Compounds **1** and **2** were purified by crystallization from methanol. All solvents (methanol, ethanol, and toluene) used in this work were purchased from Sigma-Aldrich (St. Louis, MO, USA) and POCH (Gliwice, Poland) chemical companies and were used without further purification.

Melting points were determined on a Büchi Melting Point B-540 apparatus in the capillary mode and they were uncorrected. The infrared transmission spectra of the crystalline products were recorded using a Nexus Thermo Nicolet FT-IR spectrophotometer (Wien, Austria; Faculty of Chemistry, University of Lodz). The MS-ESI were measured on Varian 500, MS LC Ion Trap mass spectrometer (Santa Clara, CA, United States; Faculty of Chemistry, University of Lodz). Elemental analyses were performed in the Faculty of Chemistry (University of Lodz) using a Vario Micro Cube (Langensfeld, Germany) by Elemental analyzer. ^1H - and ^{13}C -NMR spectra were recorded on a Bruker Avance III 600 MHz (Karlsruhe, Germany). Both samples were dissolved in DMSO deuterated. Chemical shifts

are given in ppm, coupling constants in Hz. Computational studies were used to predict the properties and future use of potential drugs. Molinspiration Cheminformatics (<http://www.molinspiration.com/products.html>) was used for the calculation of important molecular properties, molecular processing, bioactivity, and the high-quality depiction of new molecules. Molecular docking of the compounds to the HSA crystal structure 1E7I [21] was performed in AutodockVina 1.1.2 (<http://vina.scripps.edu>) [22], as previously described [12].

Lipophilicity was determined using an RP-TLC method with small amounts of organic solvents.

Assessment of erythrotoxicity of compounds **1** and **2** was made in Laboratory of Bioanalysis in the Department of Pharmaceutical Chemistry, Drug Analysis, and Radiopharmacy in the Medical University of Lodz. The erythrocyte morphology was evaluated using a phase-contrast microscope Opta-Tech (Warsaw, Poland) using the OptaView 7 programme. Biological material (blood) for research came from the Regional Blood Donation Center in Lodz.

3.1. Synthesis of (E)-3-(4-*N,N*-diethylaminobenzylidene)chroman-4-one (**1**)

A mechanically stirred mixture of 10 mmol of chroman-4-one, 10 mmol 4-*N,N*-diethylaminobenzaldehyde and five drops of piperidine was heated at 140 °C in an oil bath for 4 h. After cooling the reaction mixture was left for 24 h at room temperature. Next, methanol was added and the resulting was filtered and crystallized from methanol. Compound **1** was thus obtained as a light orange powder.

Yield: 33.5%. M.p. 124.9–125.4 °C. MS (ESI⁺): *m/z* 308. C₂₀H₂₁NO₂ [M + H]⁺. IR (KBr) ν (cm⁻¹): 3037 (C-H_{aromat}), 2968, 2923, 2895, 2870 (C-H_{aliph}), 1663 (C=O), 1600, 1584, 1524 (C=C), 1154 (C-O-C). ¹H-NMR (600 MHz, DMSO-d₆) δ (ppm): 1.12 (3H, *t*, *J*_{H-H}—6 Hz, CH₃), 3.42 (2H, *q*, *J*_{H-H}—6 Hz, CH₂), 5.45 (1H, *s*, CH), 6.75 (2H, *d*, *J*_{H-H}—6 Hz, C2-H), 7.02 (1H, *d*, *J*_{H-H}—12 Hz, C4-H_{arom}), 7.09 (1H, *t*, *J*_{H-H}—6 Hz, C6-H_{arom}), 7.32 (1H, *d*, *J*_{H-H}—6 Hz, C8-H_{arom}), 7.54 (1H, *t*, *J*_{H-H}—6 Hz, C7-H_{arom}), 7.84 (1H, *d*, *J*_{H-H}—6 Hz, C6'-H_{arom}), 7.85 (1H, *d*, *J*_{H-H}—6 Hz, C5'-H_{arom}). ¹³C-NMR (600 MHz, DMSO-d₆) δ (ppm): 12.9 (CH₂CH₃), 44.3 (CH₂CH₃), 68.4 (C-2), 111.6, 118.1, 120.8, 122.2, 122.4, 125.2 (CH_{arom}, =CH), 135.9, 133.7, 137.9, 149.2, 160.7 (C_{arom}), and 181.0 (C=O). Anal. Calc. for C₂₀H₂₁NO₂ (M = 307.386 g/mol) % C:78.14; and % H: 6.89. Found % C: 78.16; and % H: 7.06.

3.2. Synthesis of (E)-3-(4-*N,N*-diethylaminobenzylidene)-2-phenylchroman-4-one (**2**)

The compound **2** was synthesized according to Pijewska in 1993 [14]. A racemic mixture was obtained.

Yield: 34%. M.p. 170–171 °C (MeOH). MS (ESI⁺): *m/z* 384. C₂₆H₂₅NO₂ [M + H]⁺. IR (KBr) ν (cm⁻¹): 3056 (C-H_{aromat}), 2965, 2920, 2895, 2863 (C-H_{aliph}), 1654 (C=O), 1603, 1559, 1524 (C=C), 1150 (C-O-C). ¹H-NMR (600 MHz, DMSO-d₆) δ (ppm): 1.12 (3H, *t*, *J*_{H-H}—6 Hz, CH₃), 3.36 (2H, *q*, *J*_{H-H}—6 Hz, CH₂), 6.70 (1H, *s*, C2-H), 6.81–7.79 (13H, *m*, C-H_{arom}), 7.94 (1H, *s*, =CH). ¹³C-NMR (600 MHz, DMSO-d₆) δ (ppm): 12.9 (CH₂CH₃), 44.3 (CH₂CH₃), 78.1 (C2-H), 119.0, 120.2, 125.9, 127.2, 127.9, 129.1, 129.3, 136.2, 138.6, 140.3 (CH_{arom}, =CH), 122.3, 122.7, 122.7, 133.7, 149.6, 158.5 (C_{arom}), 181.2 (C=O). Anal. Calc. for C₂₆H₂₅NO₂ (M = 389.529 g/mol) % C: 81.43; % H: 6.57; % N: 3.65. Found % C: 81.57; % H: 6.78; and % N: 3.58.

3.3. Determination of Lipophilicity of Flavone Derivatives Using RP-TLC Method

The RP-TLC experiments were performed on TLC plates (5 × 10 cm) RP-18 F254S (Merck, Darmstadt, Germany). The synthesized compounds were dissolved in *N,N*-dimethylformamide DMF (2 mg/mL). High purity DMF 99.8% was obtained from Chempur (Piekary Slaskie, Poland). The solutions of each compound in DMF were spotted on plates. The spots were observed under UV light at λ = 254 nm. DMF-water solvent system was used as mobile phase. The composition of the solvent system changed from 50%:50% to 95%:5%. All experiments were performed at room temperature. The Log*P* parameter was calculated using the equation from the calibration curve.

3.4. X-ray Diffraction Experiment

The X-ray single crystal diffraction experiments for **1** and **2** were performed using an Agilent SuperNova diffractometer equipped with an Atlas detector at $T = 100(2)\text{K}$ with monochromatic $\text{MoK}\alpha$ radiation ($\lambda = 0.71073 \text{ \AA}$). Multi-scan absorption correction was applied to all data [26]. All structures were solved by direct methods using SHELX and further refined on F^2 using SHELX-2014/7 [27]. The position of the hydrogen atoms were calculated from the known geometry (C-H bond lengths at 0.93, 0.96, and 0.97 \AA for aromatic CH, methylene CH_2 , and CH_3 methyl atoms, respectively) and treated as riding, where isotropic thermal parameters of these hydrogen atoms were fixed as $U_{\text{iso}}(\text{H}) = 1.2 U_{\text{eq}}(\text{C})$ (for aromatic and methylene H atoms) or $U_{\text{iso}}(\text{H}) = 1.5 U_{\text{eq}}(\text{C})$ for (methyl H-atoms). Key experimental crystallographic data and refinement details of the studied compounds **1** and **2** are summarized in Table 5. To identify molecular geometries and hydrogen-bond patterns, PLATON and Mercury [28] were utilized. CCDC 1877734 (compound **2**) and 1877735 (compound **1**) contains the supplementary crystallographic data for this paper. These data can be obtained free of charge via www.ccdc.cam.ac.uk/data_request/cif, or by emailing data_request@ccdc.cam.ac.uk, or by contacting The Cambridge Crystallographic Data Centre, 12, Union Road, Cambridge CB2 1EZ, UK; fax: +44-1223-336-033.

Table 5. Crystal data, data collection, and refinement parameters of **1** and **2**.

	1	2
Crystal data		
Chemical formula	$\text{C}_{20}\text{H}_{21}\text{NO}_2$	$\text{C}_{26}\text{H}_{25}\text{NO}_2$
Mr	307.38	383.47
Cell setting, space group	Triclinic, $P-1$	Monoclinic, $P2_1/n$
a, b, c (\AA)	7.732(2), 13.998(2), 16.312(2)	11.764(2), 13.455(2), 12.832(2)
α, β, γ ($^\circ$)	64.74(2), 87.07(2), 87.58(2)	90.0, 93.75(2), 90.0
V (\AA^3)	1594.1(2)	2026.8(2)
Z	4	4
D_x (Mg m^{-3})	1.376	1.257
Temperature (K)	100	100
Radiation type (\AA)	0.71073	0.71073
μ (mm^{-1})	0.082	0.079
Crystal form, colour	prism, colourless	block, orange
Crystal size (mm)	$0.3 \times 0.2 \times 0.18$	$0.3 \times 0.2 \times 0.18$
Data collection		
Diffractometer	SuperNova, Atlas detector	SuperNova, Atlas detector
No. of measured and unique reflections	13098, 6603	25887, 4193
Observed data with $F^2 \geq 4\sigma(F^2)$	5664	3316
R_{int}	0.0265	0.0305
θ_{max} ($^\circ$)	26.49	26.49
Overall completeness to θ_{max} [%]	99.8	99.8
Refinement (SHELX)		
Refinement on	F^2	F^2
All data	6603	4193
R, wR [$I \geq 2(I)$]	0.0362, 0.0941	0.0513, 0.1347
R, wR (all data)	0.0434, 0.0989	0.0686, 0.1453
Goodness of fit	1.067	1.066
No. of parameters	419	268
$\rho_{\text{max}}, \rho_{\text{min}}$ ($\text{e}\text{\AA}^{-3}$)	0.249, -0.212	0.241, -0.265

3.5. Cells Cultures and Cytotoxicity Assay by MTT

Cytotoxicity was tested against human skin melanoma cells (WM-115 ECACC, Salisbury, UK), and two human leukemia cell lines—promyelocytic leukemia (HL-60) and lymphoblastic leukemia (NALM-6). The leukemia cells were cultured in RPMI 1640 medium (Invitrogen, Grand Island, NY, USA) supplemented with 10% fetal bovine serum (FBS; Invitrogen, Grand Island, NY, USA) and

gentamicin (25 µg/mL; KRKA, Slovenia). For melanoma WM-115 cells, Dulbecco's minimal essential medium (DMEM; Invitrogen, Grand Island, NY, USA) 1640 was used. Cells were grown at 37 °C in a humidified atmosphere of 5% CO₂ in air.

For all experiments, the studied compounds were dissolved in DMSO (Sigma-Aldrich, St. Louis, MO, USA) and were further diluted in a culture medium to obtain <0.1 % DMSO concentration. In each experiment control without and with 0.1% DMSO was performed.

The cytotoxicity of both compounds, and the reference compounds (4-chromanone and 3-benzylidene-flavanone) was determined by the 3-(4,5-dimethylthiazol-2-yl)-2,5-diphenyltetrazolium bromide (MTT; Sigma, St. Louis, MO, USA) assay, which measures the activity of cellular dehydrogenases [29]. Exponentially growing cells were seeded on 96-well plates (Nunc, Roskilde, Denmark). Subsequently, various concentrations of the studied compounds (freshly prepared in DMSO and diluted with complete culture medium) were added. All compounds were tested for their cytotoxicity at a final concentration of 10⁻⁷–10⁻³ M. After 46 h of incubation with the studied compounds, the cells were treated with the MTT reagent and incubation was continued for another two hours. The MTT formazan crystals were dissolved in 20% SDS (Sodium dodecyl sulphate, Sigma-Aldrich, St. Louis, USA) and 50% DMF (Sigma-Aldrich, St. Louis, MO, USA) at pH 4.7, and the absorbance was read at 570 nm on a multifunctional Victor ELISA-plate reader (Perkin Elmer, Turku, Finland). The IC₅₀ values, the concentration of the test compound, was required to reduce the cell survival fraction to 50% of the controls, and were calculated from concentration response curves and was used as a measure of the sensitivity of the cells to a given treatment. As a control, cultured cells were grown in the absence of drugs. The data points represent the means of at least five to ten repeats ± S.D (standard deviation).

3.6. Red Blood Cells Lysis Assay

The studies on biological material were approved by the Bioethics Committee of the Medical University of Lodz, Poland (RNN/27/18/KE). The blood from healthy donors (Blood Donation Centre in Lodz) was collected in tubes containing a solution of potassium EDTA. RBCs were isolated by centrifugation (3000 × g, 10 min) at 20 °C and washed three times with 0.9% saline. The studies were performed on four biological samples obtained from different blood donors.

The effects of (E)-3-(4-*N,N*-diethylaminobenzylidene)-2-phenylchroman-4-one **1** and (E)-3-(4-*N,N*-diethylaminobenzylidene)-2-phenylchroman-4-one **2** on RBCs was performed using the method described earlier [30,31]. Briefly, 2% RBCs suspension prepared in 0.9% saline was incubated at 37 °C with tested compounds added in a 10 µL volume for one hour. The percentage of solvent (methanol) did not exceed 1% of the final sample volume (1 mL). Afterwards, the samples were centrifuged at 1000 × g for 10 min (20 °C), and the absorbance of the supernatant was measured at 550 nm wavelength (spectrophotometer (Cecil CE2021, London, England)). Samples containing saline solution were used to measure spontaneous hemolysis of RBCs, while samples with Triton X-100 ((2.0% *v/v*); Polish Chemical Reagents) constituted 100% of hemoglobin release. The results are presented as a percentage of released hemoglobin. The examined concentrations of tested compounds were chosen on the basis of obtained IC₅₀ values determined for three human cancer cell lines: HL-60, NALM-6, and WM-115.

3.7. RBCs Morphology

A 2% erythrocyte suspension was incubated at 37 °C for 1 h with various concentrations of tested compounds. The morphology of the RBCs was evaluated using a phase contrast Opta-Tech inverted microscope, at 400 times magnification, equipped with image analysis software (OptaView 7).

3.8. Statistical Analysis

Statistical analysis was conducted with a commercially available package (Statistica 12.0, StatSoft). All results are presented as mean ± SD. The normality of the distribution of continuous variables was

confirmed with the Shapiro-Wilk test. Paired t-tests were used for intergroup comparisons of normally distributed variables. The results were considered significant at *p*-values lower than 0.05.

4. Conclusions

This study presents the synthesis, chemical characterization, and biological activity of 3-benzylidenederivatives of chromanone and flavanone. The structure of synthesized compounds was confirmed using NMR, MS, IR, and single crystal X-ray diffraction (XRD) techniques. The anti-cancer properties of synthesized compounds **1** and **2** were evaluated using HL-60, NALM-6, and WM-115 cancer cell lines. Both compounds exerted a greater cytotoxic effect towards all cell lines than the reference 4-chromanone and 3-benzylidene flavanone. Compound **2** exerted the most profound cytotoxic effect towards WM-115 cell line with $IC_{50} = 6.45 \pm 0.69 \mu\text{mol/L}$. Lipophilicity of both compounds was determined using an RP-TLC method. Due to the presence of a phenyl substituent in the C2 position of chromanone, the value of $\log P$ for compound **2** was higher than that for **1**. Both compounds did not affect the integrity of erythrocyte membrane over the examined concentration range and did not contribute to hemolysis. In addition, tested compounds did not induce the pathological changes in the morphology of erythrocytes since only dyscytes and echinocytes were recognized. Thus, both compounds at the concentrations close to the determined IC_{50} values might be regarded as biocompatible towards red blood cells. Computational studies suggest remarkably different ability of the synthesized compounds to bind with HSA, and different specificity as far as the future use as drugs is considered. Taking into consideration the promising cytotoxicity properties, i.e., IC_{50} values in a few micromolar range and being harmless to the red blood cells, the arylidenechromanone/flavanone derivatives can be further evaluated as promising anticancer compounds.

Supplementary Materials: Supplementary materials are available online.

Author Contributions: Conceptualization, E.B.; methodology, (Biological Assays) U.K.; (Computational Studies) M.B.P.; software (molecular modelling and docking in Vina, Molinspiration analysis, Figure 6) M.B.P.; validation, M.B.P.; formal analysis, M.M.; data curation, (molecular modelling and docking in Vina, Molinspiration analysis), M.B.P.; (X-ray experiment) M.M. and J.K.; writing—original draft preparation, (parts in introduction, computational studies, molecular modelling and docking in Vina, Molinspiration analysis) M.B.P.; (parts of introduction, X-ray analysis) M.M.; (introduction, synthesis, lipophilicity, part of biological assays, conclusions) A.A.A.-G.; (part of biological assays, conclusion) M.M.-P.; (part of biological assays, conclusion) E.B.; writing—review and editing (parts in introduction, computational studies, conclusion related to Computational Studies - molecular modelling and docking in Vina, Molinspiration analysis) M.B.P., (all text, especially X-ray structure) M.M., (all text, especially: introduction, chemistry, part of biological assays, conclusion) A.A.A.-G., (part of biological assays, conclusion) M.M.-P., (part of biological assays, conclusion) E.B.; visualization, (Figure 6) M.B.P.; (X-ray structure visualization) M.M.; (Figure 5) A.A.A.-G., (Figure 4) M.M.-P., (Scheme 1) E.B.; supervision, E.B.; project administration, A.A.A.-G., E.B.; funding acquisition, A.A.A.-G., E.B., M.M.

Funding: This research was funded by Medical University of Lodz (grant No 503/3-066-02/503-31-001, grant No 503/3-015-02/503-31-001, 503/3-015-01/503-31-004 and grant No 502-03/3-066-01/502-34-046).

Acknowledgments: Magdalena Małeczka would like to thank the University of Lodz (grant No 506/1136) for financial support.

Conflicts of Interest: The authors declare no conflict of interest.

References

1. Czaplinska, M.; Czepas, J.; Gwoździński, K. Budowa, właściwości przeciwutleniające i przeciwnowotworowe flawonoidów. *Post. Bioch.* **2012**, *58*, 235–242.
2. Nijveldt, R.J.; Van Nood, E.; Van Hoorn, D.E.; Boelens, P.G.; Van Norren, K.; Van Leeuwen, P.A. Flavonoids: A review of propable mechanisms of action and potential applications. *Am. J. Clin. Nutr.* **2001**, *74*, 418–425. [[CrossRef](#)] [[PubMed](#)]
3. Ravishankar, D.; Rajora, A.K.; Greco, F.; Osborn, H.M. Flavonoids as prospective compounds for anti-cancer therapy. *Int. J. Biochem. Cell. Biol.* **2013**, *45*, 2821–2831. [[CrossRef](#)] [[PubMed](#)]

4. Raffa, D.; Maggio, B.; Raimondi, M.V.; Plescia, F.; Daidone, G. Recent discoveries of anticancer flavonoids. *Eur. J. Med. Chem.* **2017**, *142*, 213–228. [[CrossRef](#)] [[PubMed](#)]
5. Perez-Vizcaino, F.; Fraga, C.G. Research trends in flavonoids and health. *Arch. Biochem. Biophys.* **2018**, *646*, 107–112. [[CrossRef](#)] [[PubMed](#)]
6. Sharmila, G.; Bhat, F.A.; Arunkumar, R.; Elumalai, P.; Singh, P.R.; Senthilkumar, K.; Arunakaran, J. Chemopreventive effect of quercetin, a natural dietary flavonoid on prostate cancer in in vivo model. *J. Clin. Nutr.* **2014**, *33*, 718–726. [[CrossRef](#)] [[PubMed](#)]
7. Demirayak, S.; Yurttas, L.; Gundogdu-Karaburun, N.; Karaburun, A.C.; Kayagil, I. New chroman-4-one/thiochroman-4-one derivatives as potential anticancer agents. *Saudi Pharm. J.* **2017**, *25*, 1063–1072. [[CrossRef](#)]
8. Perkin, W.H.; Ray, J.N.; Robinson, R. Experiments on the synthesis of brazilin and haematoxylin and their derivatives. Part I. Veratrylidene-7-methoxychromanone and an account of a new synthesis of some benzopyrylium salts. *J. Chem. Soc.* **1926**, *129*, 941–953. [[CrossRef](#)]
9. Levai, A.; Schag, J.B. Synthesis of 3-benzylidenechroman-4-ones and -1-thiochroman-4-ones. *Pharmazie.* **1979**, *34*, 748–749.
10. Levai, A.; Dinya, Z.; Schag, J.B.; Toth, G.; Szollosy, A. Synthesis of 3-benzyl-4-chromones and 3-benzyl-1-thio-4-chromones. *Chem. Inf.* **1981**, *36*, 465.
11. Kupcewicz, B.; Balcerowska-Czerniak, G.; Małecka, M.; Paneth, P.; Krajewska, U.; Rozalski, M. Structure-cytotoxic activity relationship of 3-arylidene flavanone and chromanone (E, Z isomers) and 3-arylflavones. *Bioorganic Med. Chem. Letters.* **2013**, *23*, 4102–4106. [[CrossRef](#)] [[PubMed](#)]
12. Budzisz, E.; Paneth, P.; Geromino, I.; Muzioł, T.; Rozalski, M.; Krajewska, U.; Pipiak, P.; Ponczek, M.B.; Malecka, M.; Kupcewicz, B. The cytotoxic effect of spiroflavanone derivatives, their binding ability to human serum albumin (HSA) and a DFT study on the mechanism of their synthesis. *J. Mol. Struct.* **1137**, 267–276. [[CrossRef](#)]
13. Teng, G.G. Negative lase sensitive lithographic printing plate having specific photosensitive composition. U.S. Patent 7,524,615, 14 February 2008.
14. Pijewska, L.; Kamecki, J.; Perka-Karolczak, W. 3-Arylidene flavanones. Part 2 Reaction with diazomethane. *Pharmazie* **1993**, *48*, 254–257.
15. Fasano, M.; Curry, S.; Terreno, E.; Galliano, M.; Narciso, G.P.; Notari, S.; Ascenzi, P. The extraordinary ligand binding properties of human serum albumin. *IUBMB Life.* **2005**, *57*, 787–796. [[CrossRef](#)] [[PubMed](#)]
16. Gangwal, R.P.; Damre, M.V.; Das, N.R.; Dhoke, G.V.; Bhadauriya, A.; Varikoti, R.A.; Sangamwar, A.T. Structure based virtual screening to identify selective phosphodiesterase 4B inhibitors. *J. Mol. Graph. Model* **2015**, *57*, 89–98. [[CrossRef](#)] [[PubMed](#)]
17. Valkonen, A.; Laihia, K.; Kolehmainen, E.; Kauppinen, R.; Perjesi, P. Structural studies of seven homoisoflavonoids, six thiohomoisoflavonoids and four structurally related compounds. *Struct. Chem.* **2012**, *23*, 209–217. [[CrossRef](#)]
18. Cremer, D.; Pople, J.A. General definition of ring puckering coordinates. *J. Amer. Chem. Soc.* **1975**, *97*, 1354–1358. [[CrossRef](#)]
19. Bhattacharya, A.A.; Grune, T.; Curry, S. Crystallographic analysis reveals common modes of binding of medium and long-chain fatty acids to human serum albumin. *J. Mol. Biol.* **2000**, *303*, 721–732. [[CrossRef](#)]
20. Duax, W.L.; Norton, D.A. *Atlas of Steroid Structure*; Springer Science & Business Media: New York, NY, USA, 2012; pp. 3273–3274.
21. Kupcewicz, B.; Małecka, M.; Zapadka, M.; Krajewska, U.; Różalski, M.; Budzisz, E. Quantitative relationships between structure and cytotoxic activity of flavonoid derivatives. An application of Hirshfeld surface derived descriptors. *Bioorg. Med. Chem. Lett.* **2016**, *26*, 3336–3341. [[CrossRef](#)]
22. Trott, O.; Olson, A.J. AutoDock Vina: Improving the Speed and Accuracy of Docking with a New Scoring Function, Efficient Optimization, and Multithreading. *J. Comput. Chem.* **2010**, *31*, 455–461.
23. Perjesi, P.; Umashankar, D.; De Clercq, E.; Balzarini, J.; Kawase, M.; Sakagami, H.; Stables, J.; Lorand, T.; Rozmer, Z.; Dimmock, J. Design, synthesis and antiproliferative activity of some 3-benzylidene-2,3-dihydro-1-benzopyran-4-ones which display selective toxicity for malignant cells. *Eur. J. Med. Chem.* **2008**, *43*, 839–845. [[CrossRef](#)]
24. Fischer, D.; Li, Y.; Ahlemeyer, B.; Krieglstein, J. In vitro cytotoxicity testing of polycations: Influence of polymer structure on cell viability and hemolysis. *Biomaterials* **2003**, *24*, 1121–1131. [[CrossRef](#)]

25. Stasiuk, M.; Kijanka, G.; Kozubek, A. Zmiany kształtu erytrocytów i czynniki je wywołujące. *Post. biochemii.* **2009**, *55*, 425–433.
26. Sheldrick, G.M. Crystal structure refinement with SHELXL. *Acta Crystallogr. Sect. Struct. Chem.* **2015**, *71*, 3–8. [[CrossRef](#)]
27. Spek, A.L. Structure validation in chemical crystallography. *Acta Cryst.* **2009**, *65*, 148–155. [[CrossRef](#)]
28. Macrae, C.F.; Bruno, I.J.; Chisholm, J.A.; Edgington, P.R.; McCabe, P.; Pidcock, E.; Rodriguez-Monge, L.; Taylor, R.; van de Streek, J.; Wood, P.A. New Features for the Visualization and Investigation of Crystal Structures. *J. App. Cryst.* **2008**, *41*, 466–470. [[CrossRef](#)]
29. Hansen, M.B.; Nielsen, S.E.; Berg, K. Re-examination and further development of a precise and rapid dye method for measuring cell growth/cell kill. *J. Immunol. Methods.* **1989**, *119*, 203–210. [[CrossRef](#)]
30. Markowicz-Piasecka, M.; Sikora, J.; Mateusiak, Ł.; Mikiciuk-Olasik, E.; Huttunen, K.M. New prodrugs of metformin do not influence the overall haemostasis potential and integrity of the erythrocyte membrane. *Eur. J. Pharm.* **2017**, *811*, 208–221. [[CrossRef](#)]
31. Markowicz-Piasecka, M.; Mikiciuk-Olasik, E.; Sikora, J. Stability of erythrocyte membrane and overall hemostasis potential—A biocompatibility study of mebrotfenin and other iminodiacetic acid derivatives. *J. Pharm. Rep.* **2015**, *67*, 1230–1239. [[CrossRef](#)]

Sample Availability: Samples of the compounds (E)-3-(4-N,N-diethylaminobenzylidene)chroman-4-one (**1**) and (E)-3-(4-N,N-diethylaminobenzylidene)-2-phenylchroman-4-one (**2**) are available from the author Angelika A. Adamus-Grabicka.



© 2018 by the authors. Licensee MDPI, Basel, Switzerland. This article is an open access article distributed under the terms and conditions of the Creative Commons Attribution (CC BY) license (<http://creativecommons.org/licenses/by/4.0/>).